Research Article Vol. 26, No. 3 | 5 Feb 2018 | OPTICS EXPRESS 2191

Optics EXPRESS

Phase retrieval in generalized optical interferometry systems

WESLEY E. FARRISS,[1,*] JAMES R. FIENUP,[1] TANYA MALHOTRA,[2] AND A. NICK VAMIVAKAS[1]

[1] *The Institute of Optics, University of Rochester, Rochester, NY, 14627, USA*
[2] *Department of Physics and Astronomy, University of Rochester, Rochester, NY, 14627, USA*
[*] *wfarriss@gmail.com*

Abstract: Modal analysis of an optical field via generalized interferometry (GI) is a novel technique that treats said field as a linear superposition of transverse modes and recovers the amplitudes of modal weighting coefficients. We use phase retrieval by nonlinear optimization to recover the phase of these modal weighting coefficients. Information diversity increases the robustness of the algorithm by better constraining the solution. Additionally, multiple sets of random starting phase values assist the algorithm in overcoming local minima. The algorithm was able to recover nearly all coefficient phases for simulated fields consisting of up to 21 superpositioned Hermite Gaussian modes from simulated data and proved to be resilient to shot noise.

OCIS codes: (070.2575) Fractional Fourier transforms; (100.5070) Phase retrieval; (200.4740) Optical processing; (010.7350) Wave-front sensing; (120.3180) Interferometry.

References and links

1. N. Riesen and J. D. Love, "Design of mode-sorting asymmetric y-junctions," Appl. Opt. **51**, 2778–2783 (2012).
2. M. Malik, M. O'Sullivan, B. Rodenburg, M. Mirhosseini, J. Leach, M. P. J. Lavery, M. J. Padgett, and R. W. Boyd, "Influence of atmospheric turbulence on optical communications using orbital angular momentum for encoding," Opt. Express **20**, 13195–13200 (2012).
3. M. N. O'Sullivan, M. Mirhosseini, M. Malik, and R. W. Boyd, "Near-perfect sorting of orbital angular momentum and angular position states of light," Opt. Express **20**, 24444–24449 (2012).
4. P. Villoresi, T. Jennewein, F. Tamburini, M. Aspelmeyer, C. Bonato, R. Ursin, C. Pernechele, V. Luceri, G. Bianco, A. Zeilinger , "Experimental verification of the feasibility of a quantum channel between space and earth," New J. Phys. **10**, 033038 (2008).
5. M. Krenn, J. Handsteiner, M. Fink, R. Fickler, and A. Zeilinger, "Twisted photon entanglement through turbulent air across vienna," P. Natl. Acad. Sci. USA **112**, 14197–14201 (2015).
6. A. F. Abouraddy, T. M. Yarnall, and B. E. A. Saleh, "Generalized optical interferometry for modal analysis in arbitrary degrees of freedom," Opt. Lett. **37**, 2889–2891 (2012).
7. A. F. Abouraddy, T. M. Yarnall, and B. E. Saleh, "Angular and radial mode analyzer for optical beams," Opt. Lett. **36**, 4683–4685 (2011).
8. J. A. Rodrigo, T. Alieva, and M. L. Calvo, "Programmable two-dimensional optical fractional Fourier processor," Opt. Express **17**, 4976–4983 (2009).
9. D. Mardani, A. F. Abouraddy, and G. K. Atia, "Efficient modal analysis using compressive optical interferometry," Opt. Express **23**, 28449–28458 (2015).
10. B. H. Dean, D. L. Aronstein, J. S. Smith, R. Shiri, and D. S. Acton, "Phase retrieval algorithm for JWST flight and testbed telescope," in "SPIE Astronomical Telescopes+ Instrumentation," (International Society for Optics and Photonics, 2006), pp. 626511.
11. D. L. Aronstein, J. S. Smith, T. P. Zielinski, R. Telfer, S. C. Tournois, D. B. Moore, and J. R. Fienup, "Wavefront-error performance characterization for the James Webb Space Telescope (JWST) integrated science instrument module (isim) science instruments," in "SPIE Astronomical Telescopes+ Instrumentation," (International Society for Optics and Photonics, 2016), pp. 990409.
12. R. P. Millane, "Phase retrieval in crystallography and optics," J. Opt. Soc. Am. A **7**, 394–411 (1990).
13. L.-H. Yeh, J. Dong, J. Zhong, L. Tian, M. Chen, G. Tang, M. Soltanolkotabi, and L. Waller, "Experimental robustness of Fourier ptychography phase retrieval algorithms," Opt. Express **23**, 33214–33240 (2015).
14. J. R. Fienup, "Phase retrieval algorithms: a comparison," Appl. Opt. **21**, 2758–2769 (1982).
15. C. Fienup and J. Dainty, "Phase retrieval and image reconstruction for astronomy," Image Recovery: Theory and Application pp. 231–275 (1987).

#305707 https://doi.org/10.1364/OE.26.002191
Journal © 2017 Received 26 Sep 2017; revised 10 Dec 2017; accepted 16 Dec 2017; published 22 Jan 2018

16. M. Guizar-Sicairos and J. R. Fienup, “Phase retrieval with transverse translation diversity: a nonlinear optimization approach,” Opt. Express **16**, 7264–7278 (2008).
17. O. Shapira, A. F. Abouraddy, J. D. Joannopoulos, and Y. Fink, “Complete modal decomposition for optical waveguides,” Phys. Rev. Lett. **94**, 143902 (2005).
18. B. M. Hennelly and J. T. Sheridan, “Generalizing, optimizing, and inventing numerical algorithms for the fractional Fourier, Fresnel, and linear canonical transforms,” J. Opt. Soc. Am. A **22**, 917–927 (2005).
19. M. A. Alonso, “Wigner functions in optics: describing beams as ray bundles and pulses as particle ensembles,” Advances in Optics and Photonics **3**, 272–365 (2011).
20. H. M. Ozaktas, Z. Zalevsky, and M. A. Kutay, *The Fractional Fourier Transform: with Applications in Optics and Signal Processing*, 1st ed. (Wiley, 2001).
21. A. Siegman, *Lasers* (University Science Books, 1986).
22. J. Nocedal and S. J. Wright, *Numerical Optimization* (Springer, 2006), 2nd ed.
23. E. Jones, T. Oliphant, P. Peterson *et al.*, “SciPy: Open source scientific tools for Python,” (2001). [Online; accessed March 10, 2016].
24. A. S. Jurling and J. R. Fienup, “Applications of algorithmic differentiation to phase retrieval algorithms,” J. Opt. Soc. Am. A **31**, 1348–1359 (2014).
25. J. Fienup and C. Wackerman, “Phase-retrieval stagnation problems and solutions,” J. Opt. Soc. Am. A **3**, 1897–1907 (1986).
26. M. Guizar-Sicairos and J. R. Fienup, “Understanding the twin-image problem in phase retrieval,” J. Opt. Soc. Am. A **29**, 2367–2375 (2012).

---

1. Introduction

Methods which analyze modal coefficients of fields have been studied using a variety of different techniques. Historically, much of the modal analysis work has been associated with sorting fields propagated through multimodal fibers for use in optical communication systems [1]. Recently however, there has been a great deal of focus on analyzing propagated, freespace fields into a transverse basis set for use in both satellite and terrestrial-based communication systems [2–4]. Experimental recovery of messages encoded in the relative phase between two superpositioned freespace modes has also been conducted over long propagaton distances through atmospheric turbulence using machine learning techniques [5].

In this paper, we describe a phase retrieval algorithm for a novel interferometry system known as a generalized optical interferometer. By itself, this system enables one to analyze a monochromatic, scalar optical field propagated through free-space. By considering the field transiting through the interferometer as a weighted superposition of Hermite Gaussian (HG) modes, the system is able to recover the amplitudes of the generally complex-valued weighting coefficients [6, 7]. This interferometer uses generalized phase operators (GPOs) which, for cases of concern here, conducts a fractional Fourier transform (fFT) with respect to one or both transverse beam dimensions of the input field. The optical elements that conduct the fFTs are balanced with the beam parameters such that the diameter of the system’s output intensity distribution never changes, regardless of the GPO encoding [8]. This is accomplished without physically repositioning any optical elements in the system. The recovery of the amplitudes will be described briefly in Section 2. An additional approach to amplitude recovery can also be found in [9]. After the amplitude of each coefficient is recovered, we wish to recover the phase of these coefficients. Phase retrieval techniques have been used in a variety of applications including wave-front sensing [10], metrology [11], crystallography [12], microscopy [13], astronomical speckle imaging [14, 15], x-ray diffraction imaging [16], and decomposition of TEM modes in multimodal fibers [17]. Section 3 describes our novel nonlinear optimization-based phase retrieval algorithm. Section 4 describes and gives results for Monte Carlo simulations that were conducted to characterize the algorithm and provides best practices for its use. Section 5 draws conclusions and discusses future work motivated by the results in Section 4.

2. Generalized optical interferometry theory

2.1. Generalized optical interferometry basics

In a generalized optical interferometer (GI) , GPOs are added in one or more arms of an interferometer (in this case a Mach-Zehnder type). GPOs take the form of a transform kernel associated with a manipulation of a physical property of the optical field. These properties include phase, polarization, temporal delay, parity (flipping of the field as in a dove prism), etc. [6]. In this work, we confine our investigation to a specific type of GPO whose only effect on the field is to add a known phase to the field. Each term in the linear combination that describes the original field is a weighted member of a basis set. The members of the basis set when operated on by the GPO produce a phase-only eigenvalue: given a transverse scalar field,

$$U(x, y) = \sum_n c_n \psi_n(x, y), \tag{1}$$

a GPO, Λ_α, is defined such that,

$$\Lambda_\alpha \{U(x, y)\} = \sum_m c_m e^{\frac{im\pi\alpha}{2}} \psi_m(x, y), \tag{2}$$

where α is the transform parameter of the GPO.

An operator and basis set combination that exhibit the desired functionality are the fractional-Fourier Transform and Hermite Gaussian (HG) basis set. The fFT is a linear canonical transform whose effect on the phase-space distribution of a transverse field distribution is a rotation of the rectangular region whose area is the space-bandwidth product of a single dimension [18, 19] . A $\pi/2$ radian rotation of this rectangular region in phase space corresponds to a Fourier transform and a $-\pi/2$ radian rotation corresponds to an inverse Fourier transform. Rotations that are not discrete multiples of $\pi/2$ radians are "fractions" of a full Fourier transform and are thus referred to as fractional Fourier transforms. The order of an fFT, α, corresponds to the amount of rotation in phase space imparted by the transform. An fFT can also be thought of as a propagator similar to a Fresnel transform in that it can be used to conduct a propagation from the exit pupil of the system to any other plane [20]. In this paper, if θ is the phase space rotation in radians, the fFT will be represented as $\mathcal{F}_\alpha\{\cdot\}$, where $\alpha = 2\theta/\pi$. So the first Fourier transform plane is at $\alpha = 1$, which corresponds to a $\pi/2$ rotation in phase space. The fFT is a periodic operator in the sense that the operation performed at α is the same as the operation performed at $\alpha + 4p$ where p is any integer. The symbols $\mathcal{F}\{\cdot\}$ and $\mathcal{F}^{-1}\{\cdot\}$, without an α value, will represent a standard Fourier transform and inverse Fourier transform, respectively. HG modes are defined at the beam waist in two dimensions as

$$HG_{mn}(x, y) = H_m\left(\frac{\sqrt{2}x}{w_0}\right) H_n\left(\frac{\sqrt{2}y}{w_0}\right) \exp\left[\frac{-(x^2+y^2)}{w_0^2}\right], \tag{3}$$

where H_m and H_n are physicist's Hermite polynomials of order m and n, respectively, and w_0 is the radius of the beam waist. They are well known solutions to the paraxial wave equation [21]. Throughout this paper HG mode superpositions will be referred to by order. The ℓ^{th} order of HG modes is inclusive of all modes such that the indices m and n in a given mode, HG_{mn}, satisfy the condition $m + n \leq \ell$.

2.2. Generalized Mach-Zehnder Interferometry

In this work, a Mach-Zehnder interferometer (MZI), as shown in Fig. 1, was used. Each arm of the interferometer holds a GPO as described by Eq. (2). The upper output port of the interferometer

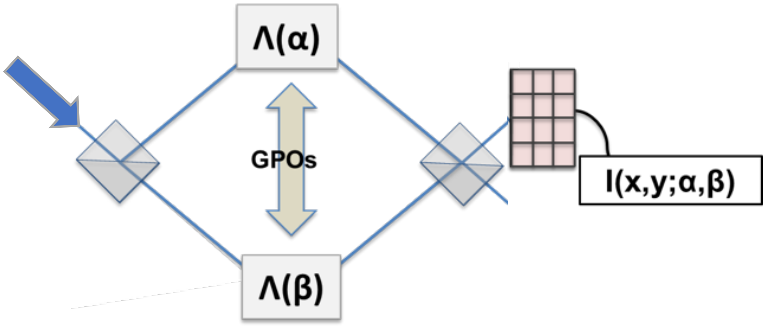

Fig. 1. Mach-Zehnder generalized interferometer configuration used for phase retrieval simulations. The array detector placed at the upper port of the figure also functions as a bucket detector for GOI amplitude recovery by integrating over all pixels

contains an array detector which, when used to recover $|c_{mn}|$ values, will function as a bucket detector by integrating over all pixels. When used to retrieve ϕ_{mn} values, the pixel information will be used normally, i.e. the pixel energies will not be integrated [6,9]. This spatial information is used in the phase retrieval process.

Using Eq. (2), the field exiting the upper output port of the interferometer is

$$\begin{aligned} U_{out}(x,y;\alpha,\beta) &= \frac{1}{\sqrt{2}}\left[\Lambda_\alpha + \Lambda_\beta\right] U_{in}(x,y) = \frac{1}{\sqrt{2}}\left[\Lambda_\alpha + \Lambda_\beta\right] \sum_{m,n} c_{mn} HG_{mn}(x,y) \\ &= \frac{1}{\sqrt{2}} \sum_{m,n} c_{mn} \left[e^{\frac{im\pi\alpha}{2}} HG_{mn}(x,y) + e^{\frac{in\pi\beta}{2}} HG_{mn}(x,y) \right] \\ &= \frac{1}{\sqrt{2}} \sum_{m,n} c_{mn} HG_{mn}(x,y) \left(e^{\frac{im\pi\alpha}{2}} + e^{\frac{in\pi\beta}{2}} \right). \end{aligned} \tag{4}$$

where Λ_α and Λ_β are the GPOs in the upper and lower arms of the interferometer, respectively.

The intensity at the output port of the MZI with the bucket detector is

$$\begin{aligned} I_{out}(x,y;\alpha,\beta) &= \left| \frac{1}{\sqrt{2}} \sum_{m,n} c_{mn} HG_{mn}(x,y) \left(e^{\frac{im\pi\alpha}{2}} + e^{\frac{in\pi\beta}{2}} \right) \right|^2 \\ &= \frac{1}{2} \left\{ \sum_{m,n} |c_{mn}|^2 HG^2_{mn}(x,y) \left[2 + 2\cos\left(\frac{m\pi\alpha}{2} - \frac{n\pi\beta}{2} \right) \right] \right. \\ &\quad + \left[\sum_{\substack{m,n;m',n' \\ m,n \neq m',n'}} c_{mn} c^*_{m',n'} HG_{mn}(x,y) HG_{m'n'}(x,y) \right. \\ &\quad \left. \left. \times \left(e^{\frac{im\pi\alpha}{2}} + e^{\frac{in\pi\beta}{2}} \right) \left(e^{-\frac{im'\pi\alpha}{2}} + e^{-\frac{in'\pi\beta}{2}} \right) \right] \right\}. \end{aligned} \tag{5}$$

The bucket detector integrates over the transverse spatial dimensions x and y. Using the orthogonality relation of HG modes,

$$\iint_{\infty}^{\infty} dxdy HG_{mn}(x,y) HG_{m'n'}(x,y) = S(m,n)\delta_{mm'}\delta_{nn'}, \tag{6}$$

where δ is the Kroenecker delta function, the signal measured by the bucket detector is:

$$\begin{aligned} P_{out}(\alpha,\beta) &= \iint dxdy I_{out}(x,y;\alpha,\beta) \\ &= \sum_{m,n} |c_{mn}|^2 \left[1+\cos\left(\frac{m\pi\alpha}{2}-\frac{n\pi\beta}{2}\right)\right] S(m,n). \end{aligned} \tag{7}$$

For convenience, we assume HG mode energy is unit normalized, i.e. $S(m,n) = 1$. The bias term can be removed from the interferogram. Since $P_{out}(0,0) = 2\sum_{mn}|c_{mn}|^2$, its measurement can be used in a well calibrated system to remove the bias term as follows:

$$\begin{aligned} P'_{out}(\alpha,\beta) &= P_{out}(\alpha,\beta) - \sum_{mn}|c_{mn}|^2 \\ &= \sum_{mn}|c_{mn}|^2 \cos\left(\frac{m\pi\alpha}{2}-\frac{n\pi\beta}{2}\right). \end{aligned} \tag{8}$$

For simplicity, assume that we are able to sample $P_{out}(\alpha,\beta)$ finely enough in α and β to approximate a continuous function space. The Fourier transform of $P'_{out}(\alpha,\beta)$ to a continuous m', n' space is

$$\begin{aligned} \tilde{P'}_{out}(m',n') &= \mathcal{F}\{P'_{out}(\alpha,\beta)\}_{\{\alpha,\beta\}\to\{m',n'\}} \\ &= \sum_{m,n}|c_{mn}|^2 \mathcal{F}\left\{\cos\left(\frac{m\pi\alpha}{2}-\frac{n\pi\beta}{2}\right)\right\} \\ &= \sum_{m,n}|c_{mn}|^2 \left[\delta\left(m'-\frac{m}{4}, n'+\frac{n}{4}\right)+\delta\left(m'+\frac{m}{4}, n'-\frac{n}{4}\right)\right]. \end{aligned} \tag{9}$$

So the recovery of the amplitude coefficients is conceptually just a matter of measuring the intensities of the δ-function peaks in $P'(m',n')$. The δ-function offset as a factor of $1/4$ is the result of the frequency modulation terms $\alpha\pi/2$ and $\beta\pi/2$ in the cosine function. The δ-function would instead peak at integer values if these terms were instead $2\alpha\pi$ and $2\beta\pi$. More detailed explanations of amplitude coefficient recovery which account for sampling in discrete spaces can be found in [9].

3. Phase retrieval in generalized Mach-Zehnder interferometer

To characterize a monochromatic scalar field described as a linear superposition of HG modes, both the phase and amplitude of the complex-valued weighting coefficients, $c_{mn} = |c_{mn}|e^{i\phi_{mn}}$, must be determined. Nominally, the amplitude information of the field, $|\vec{c}| = \{c_{mn}\}$, has been successfully recovered using the GI. Now $\vec{\phi}$ must be recovered.

Given the intensity distribution given by Eq. (5) from the lower output port of the interferometer and previously recovered amplitude coefficients, we seek to solve the inverse problem of retrieving the phases, $\vec{\phi} = \{\phi_{mn}\}$, associated with each amplitude coefficient. This can be cast as a nonlinear optimization problem where the error metric to be minimized is

$$E = \sum_{x,y}\left|I_{\mathrm{est}}\left(x,y;\alpha,\beta;\hat{\vec{\phi}}\right) - I_{\mathrm{d}}\left(x,y;\alpha,\beta\right)\right|^2, \tag{10}$$

where $I_{\mathrm{d}}(x,y)$ is the measured detector intensity in the upper output of the interferometer and

$$I_{\mathrm{est}}(x,y;\alpha,\beta;\hat{\vec{\phi}}) = \frac{1}{2}\left|\sum_{mn}|c_{mn}|HG_{mn}(x,y)e^{i\hat{\phi}_{mn}}\left(e^{\frac{im\pi\alpha}{2}}+e^{\frac{in\pi\beta}{2}}\right)\right|^2. \tag{11}$$

is an estimated intensity distribution computed from $\hat{\vec{\phi}}$, an estimate of $\vec{\phi}$.

Note that, based on the intensity model in Eq. (11), there exist values where certain modes will be suppressed from the output intensity of the interferometer. Any time that $\exp(im\pi\alpha/2) + \exp(in\pi\beta/2) = 0$, the mode HG_{mn} will not contribute to the output intensity. For example, in the case of an inverted image transform, $\alpha = \beta = 2$, any modes where $m + n$ is an odd whole number will result in an intensity plane that contains no contribution from HG_{mn}. Hence, α, β plane selections where there are suppressed modes cannot retrieve the phases of those suppressed modes. Fortunately, values of α and β can be chosen that do not suppress modes. Moreover, multiple intensity planes, each with different values of α and β, can be used to add robustness and overcome mode suppression, as will be described later.

To retrieve $\vec{\phi}$ we employed the LBFGS [22] algorithm from the scipy.optimize.minimize package from `http://scipy.org` [23]. The LBFGS was supplied an initial phase estimate of $\hat{\vec{\phi}}_{\text{init}}$ drawn from a uniform random distribution and was allowed to iterate until the error metric value reached a minimum. It is worth noting that the ability to express propagation as a trivially parallelizable series of scalar multiplications, instead of a traditional DFT(discrete Fourier transform)-based transform (or FFT), means that it has a very low computational cost when compared to most other phase retrieval algorithms that rely on DFTs (or FFTs) in both the optimization's forward and reverse model [24].

The optimization process described above does not always yield the desired phase values. There are two common failure modes for this process. The first failure mode occurs when the derivative information guides the optimizer into a local minimum of the error metric. The second common failure mode occurs due to what we call a "twin image" problem [25, 26] although that is a misnomer in this work. It is the result of a degeneracy introduced because Eq. (11) actually has two global minima, because of the modulus operation. One of these global minimums will yield the correct relative phases. The other global minimum, generally, will not.

The twin image failure case is eliminated by adding information diversity to the optimization in the form of measurements of one or more additional planes of intensities, each with different α, β values. As the GI is designed to sweep through values of α and β in order to build $P'_{out}(\alpha, \beta)$, more than one plane of spatially resolved intensities, $I_d(x, y; \alpha, \beta)$ can be measured by the detector array. This is akin to information-diverse phase retrieval techniques such as defocus-diverse phase retrieval [10] and transverse-translation-diverse phase retrieval [16]. The aggregate objective function is then

$$E_{agg} = \sum_{\{\alpha,\beta\}} E(\{\alpha, \beta\}) = \sum_{\{\alpha,\beta\}} \sum_{x,y} \left| I_{est}\left(x, y; \alpha, \beta; \hat{\vec{\phi}}\right) - I_d(x, y; \alpha, \beta) \right|^2 . \tag{12}$$

So in multiple-plane cases, the "twin-image" is eliminated because the degenerate global minimum of the error metric with respect to $\vec{\phi}$ at one α, β intensity plane will not be a global minimum for intensity planes with different α, β values. Furthermore, adding a greater diversity of information to a nonlinear optimization-based phase retrieval algorithm has been shown to increase the rate of successful retrieval in terms of convergence to the global minimum and resistance to measurement noise.

4. Simulations

Simulation experiments were conducted to test the performance of the approach. Simulations were always conducted over many different fields (i.e. the fields were generated using different random $|\vec{c}|$ and $\vec{\phi}$ values) to ensure that success or failure is agnostic of the particular field being retrieved. Intensities were generated as superpositions of unit-normalized HG modes, centered at the beam waist (HG modes are real valued at the beam waist). Modes were well oversampled in 256×256 pixel arrays with pixel spacings $\delta x,\ \delta y = w_0/32$, where w_0 is the radius of the beam at the waist. Coefficient amplitudes were assumed to be known in advance of initiating the phase retrieval process, since they would be available from the analysis of $\tilde{P}'_{out}(m', n')$ data. Unless otherwise stated explicitly, all simulations were conducted for superpositions of 2nd order (3 modes) through 6th order (21 modes) HG modes. The metric for success in all cases was an error of retrieved relative phase values with respect to the true phase values of < 0.07 waves RMS. As in wave-front sensing phase retrieval, only the relative phases can be recovered. So, the recovered phase values likely will differ from the actual phase values by a global piston phase.

4.1. *Single-plane phase retrieval*

The first test of the phase retrieval algorithm was to see if it was possible to retrieve phase from only a single spatially distributed intensity in the $\alpha = \beta = 0$ plane. This plane is representative of the intensity of the field in the interferometer without any operation being executed on the field. Twenty random fields were generated for each order ℓ. Fifty retrieval attempts were made for each of those twenty fields (a total of one thousand retrieval attempts at each order). All 50 retrieval attempts for a single field used a different random starting guess, $\hat{\vec{\phi}}_{init}$. Note that the random starting points were seeded and each one of the twenty fields used the same 50 random starting points. As seen in Table 1, a greater number of modes corresponded to a smaller fraction of successes, as one would expect. The algorithm converged to “twin-image" solutions about as often as it converged to the true solution. All non-“twin-image" failures resulted from optimizer stagnation at a local minima.

Table 1. **Success of single $\alpha = \beta = 0$ plane GI phase retrieval**

HG order	# Modes	% Success	% Twin Image
$\ell = 2$	3	46.7	44.6
$\ell = 3$	6	37.1	34.5
$\ell = 4$	10	31.4	27.4
$\ell = 5$	15	23.1	22.8
$\ell = 6$	21	22.6	24.4
$\ell = 7$	28	18.1	19.1
$\ell = 8$	36	14.3	14.5
$\ell = 9$	45	10.9	10.4
$\ell = 10$	55	10.6	10.0
$\ell = 11$	66	9.8	10.0

Next, retrievals were conducted with varying α and β values applied to the input field of the interferometer. α and β were sampled in twenty-five equally spaced increments from 0 to 2. Ten random fields were generated for each order ℓ and α, β combination. Retrieval of each field was attempted with five random $\hat{\vec{\phi}}_{init}$ starting guesses. With the exception of planes where retrieval failed due to mode suppression (see Section 3), no trend is seen that indicates a certain range of α, β values will yield a significantly greater number of successes than any other. Success rates for single-plane phase retrieval where α and β are varied do not change demonstrably from success rates where $\alpha = \beta = 0$. Single-plane success rates are shown in the bottom curve of Fig. 2, which treats the results of each $\hat{\vec{\phi}}_{init}$ separately. Given the twin image problem, around 50% is generally the highest success rate possible for the single-plane phase retrieval with a single $\hat{\vec{\phi}}_{init}$. If however we allow up to five different $\hat{\vec{\phi}}_{init}$ guesses for a single-plane phase retrieval, the success rates increased to 94% for 2nd order, 83% for 3rd order, 78% for 4th order, and 77% for 5th and 6th orders.

4.2. *Two-plane phase retrieval*

In the next round of simulations, additional planes of intensity information were added in order to further constrain the nonlinear optimization, which includes the ability to overcome the twin image problem. These Monte Carlo studies were conducted to determine if any specific combinations of α, β intensity planes yielded significantly improved success rates for retrieval. For simplicity, we held $\alpha = \beta$, thereby reducing computational requirements for the Monte Carlo study.

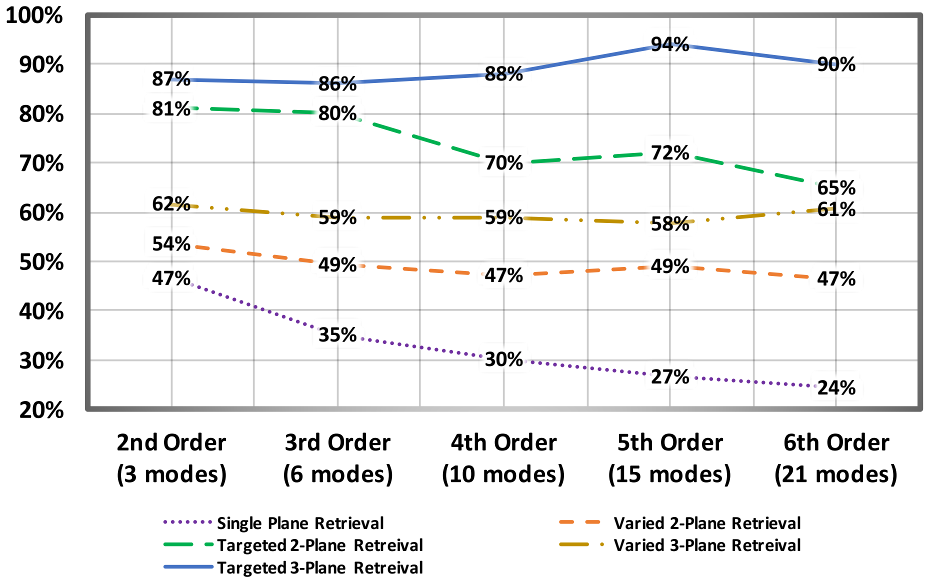

Fig. 2. Chart compares percent of successful retrievals for single-plane, two-plane, two-plane targeted, three-plane, and three-plane targeted phase retrieval techniques using only a single set of $\hat{\vec{\phi}}_{init}$ starting values.

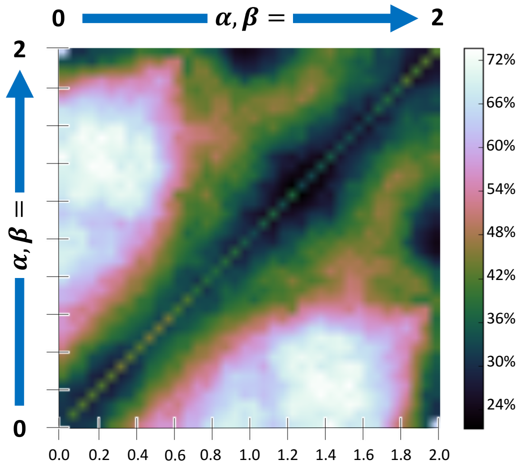

Fig. 3. Heatmap of successful retrieval rates as a function of α, β values for two-plane GI phase retrieval with 10 modes (4th order).

Runs were conducted for HG superpositions consisting of modes for orders from $\ell = 2$ through $\ell = 6$. Forty evenly-spaced α, β planes, with α, β values between $[0, 2]$ were used. Optimizations were performed for twenty different fields at every combination of these forty different α, β values. Retrieval of each of these twenty fields was conducted using fifty different $\hat{\vec{\phi}}_{init}$ starting guesses. A heat map of the success rates for order $\ell = 4$ (10 superpositioned modes) is shown in Fig. 3. A preference is seen for plane combinations where the α, β values for one plane are between 0.2 and 0.4 and the other plane has α, β between 1.4 and 1.6. Similar preferred plane combinations were seen for all HG orders tested. We suspect this preference might be due to planes in these regions having the greatest amount of unique information to constrain the problem and containing the fewest suppressed modes.

Having located preferential α, β ranges, we conducted tests to determine the performance of the algorithm for these preferred values. Monte Carlo simulations were run for α, β planes in the targeted regions for 50 additional randomly generated fields. In each optimization, α, β values were chosen randomly from the ranges in column 4 of Table 2. Using a single random $\hat{\vec{\phi}}_{init}$, the percentage of phases retrieved successfully are included percent of optimizations retrieved successfully are shown in column 3 of Table 2. With two well-chosen planes, a similar fraction of successful retrievals were obtained up to 21 modes (6^{th} order).

Table 2. **Success rates of two α, β plane GI phase retrieval**

HG order	# Modes	% Success	(α, β) Range
$\ell = 2$	3	81	(0.1, 0.3), (1.4, 1.6)
$\ell = 3$	6	80	(0.1, 0.3), (1.2, 1.4)
$\ell = 4$	10	70	(0.1, 0.3), (1.2, 1.4)
$\ell = 5$	15	72	(0.1, 0.3), (1.4, 1.6)
$\ell = 6$	21	65	(0.1, 0.3), (1.2, 1.4)

4.3. Three-plane phase retrieval

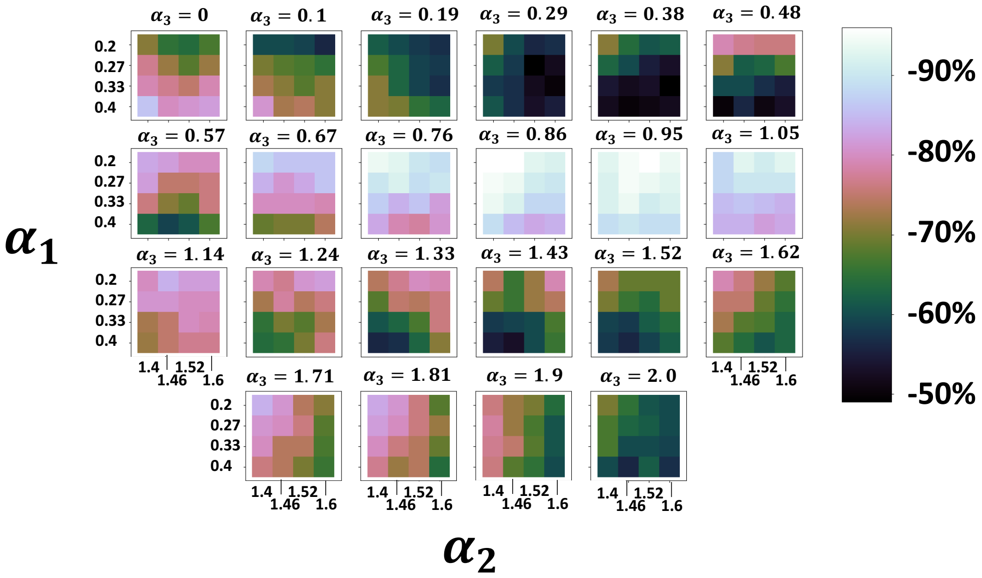

Fig. 4. Heatmaps detail success of three-plane phase retrieval of a 6^{th} order superposition with 22 equally-spaced values of α in the third plane.

With the increased success of the two-plane phase retrievals, a third plane was added in an attempt to further improve rate of successful retrieval with a single $\hat{\vec{\phi}}_{init}$ starting guess. To simulate this, the range of the fFT orders was limited to $[0.2 - 0.4]$ for the first plane and $[1.4 - 1.6]$ for the second plane, each in range sampled in 4 equally-spaced increments. The third plane was allowed to vary from order $\alpha = \beta = 0$ to $\alpha = \beta = 2$, in 22 equally spaced intervals. The percentage of successful retrievals with respect to the α-value of three intensity planes used is shown in Fig. 4. The best success rates are seen for a third fFT plane whose α, β in the range $[0.72, 1.04]$. This range is roughly equidistant from the regions of the first two planes. This would be in line with our earlier speculation that the preferred planes will occur in the regions that provide the optimizer with the most unique information. The rate of successful retrievals with intensity plane combinations in this range are consistently greater than 90% for a single $\hat{\vec{\phi}}_{init}$. No obvious trend was observed, with respect to amplitude and phase values, that would imply that certain values of coefficient phases and amplitudes, or combinations thereof, caused more failures or successes than any others. In Fig. 2 there are a few cases where a greater number of modes experienced a greater percentage of overall successes. This is most likely due to the randomness of the fields generated and the start points used in retrieval attempts. Given a large enough sample of randomly generated fields and random starting points, we expect the percentage of success will be monotonically decreasing as the number of modes present in the superposition increases. It is worth noting that the process for choosing the α, β range for the three plane superposition may not be ideal. The best way to determine the most ideal three plane combination would be to conduct a Monte Carlo simulation allowing the α, β values for all three planes to vary simultaneously. We chose not to use this process because of the time and resources needed to conduct a Monte Carlo simulation in this way and because the method we did use to determine preferential α, β values was more than sufficient to create a robust algorithm.

4.4. *Final algorithm performance*

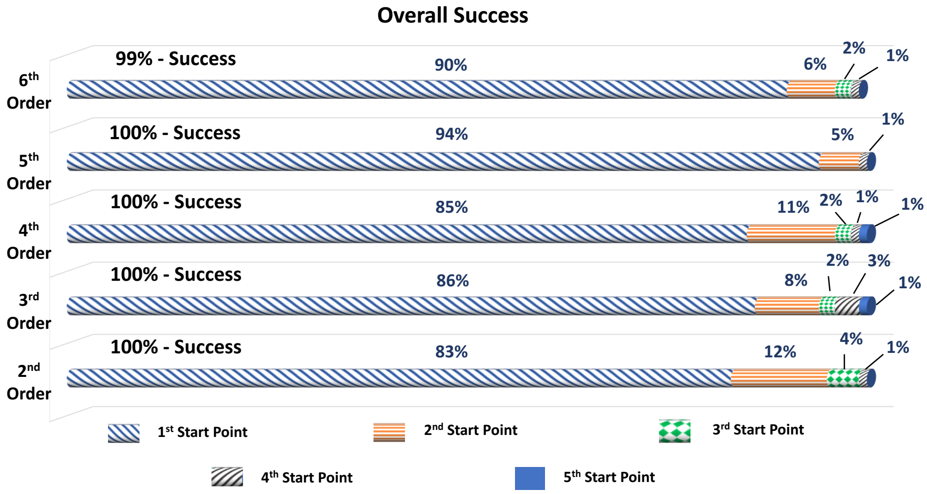

Fig. 5. Percent successful retrievals when three targeted α planes and 5 random starting sets of phase values are permitted (noiseless).

With success rates consistently greater than 85% achieved in the three-plane retrievals for a single $\hat{\vec{\phi}}_{init}$, the algorithm was deemed effective and final performance runs with targeted plane selections were conducted. For each set of simulated data, the algorithm was permitted a maximum of 5 attempts, with different $\hat{\vec{\phi}}_{init}$, to retrieve the correct phase. Phase retrieval was attempted for 100 random fields for each order. The results of this final algorithm, with a breakdown of success by starting-guess number, are shown in Fig. 5. It shows that if the algorithm fails with the first random starting guess, the second starting guess was successful the majority of the time. Almost 100% of cases succeeded using up to 5 starting points. For real world application where one cannot check the algorithm against the known phase values, the error metric is more than sufficient to identify successes and failures for the fields we retrieved. The smallest average

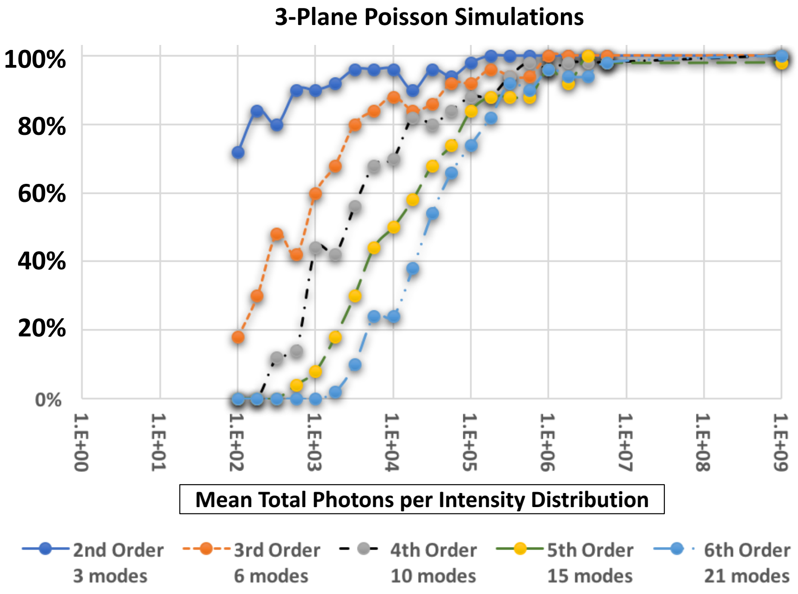

Fig. 6. Variability in percentage success with final algorithm when in the presence of limited photon budget and Poisson noise.

error metric separation between failed retrievals and successful retrievals occurred in the 4th order superpositions where the average error metric of a failed retrieval was greater than 10^{-5} while average error metric value for successful retrievals was less than 10^{-20} for this noise-free case.

Additionally, runs were conducted where reference intensities subjected to Poisson noise, each with a different total number of photons, in order to test the robustness of the algorithm and SNR requirements for good performance. Again, up to 5 $\hat{\hat{\phi}}_{init}$ were allowed for each attempted retrieval for three targeted intensity planes in the preferential α-value regions established in earlier simulations. The average number of total photons per intensity over the 256×256 pixel array varied from 10^2 to 10^7. The exponent determining the average number of total photons varied in 21 equally spaced values from 2 to 7. Fig. 6 shows the results: Nearly all phases were correctly retrieved at 10^7 average total photons per intensity plane and greater than 90% of all phases were retrieved at 10^6 average total photons per intensity, for up to 6^{th} order superpositions. Superpositions composed of fewer modes are generally more successful, especially for low SNRs. For example, at 10^3 average total photons per intensity plane, 90% of 2^{nd} order superposition phases were recovered successfully whereas no 6^{th} order superposition phases were recovered successfully. When the average total photons increased to 10^4, 25% of phases were recovered at 6^{th} order and 96% all 2^{nd} order superposition phases were recovered successfully.

5. Conclusion

It has been shown in this work that coefficient phases of a linear comination of scalar monochromatic Hermite Gaussian modes operated on by a generalized interferometer can be recovered using nonlinear optimization-based phase retrieval. This phase retrieval requires information diversity in the form of a small number of spatially resolved intensity plane measurements (1-3 array detector planes) to sufficiently constrain the problem. A clear preference for combining certain orders of fFT intensity planes has been shown. A modest number of random starting guesses for phase values are used to aid in overcoming local minima. Phase has been successfully recovered from field simulations consisting of up to 66 superposed HG modes. Additionally, this phase retrieval technique has been shown to be robust to Poisson noise.

Follow-up work will consist of retrieving phase from actual laboratory data derived from a GI. Also, phase retrieval without spatial detector information will be pursued in order to enable the resulting system to function using only a bucket detector with a goal of greatly increasing the speed of detection and usefulness in the low-photon regime, thereby increasing the overall versatility of the GI system.

Funding

U. S. Navy Office of Naval Research (N00014-14-1-0260